Synthesis and Dynamic Behavior of Mercury-Linked Clusters Containing Methoxymethylidyne Ligands: X-ray Structures of $Hg[Fe_2M(\mu_3\text{-}COCH_3)(CO)_7(\eta\text{-}C_5H_5)]_2$ (M = Co, Rh), $Hg[Ru_3(\mu\text{-}COCH_3)(CO)_{10}]_2$, and $Hg[Fe(CO)_4(\mu\text{-}Hg)Fe_3(\mu\text{-}COCH_3)(CO)_{10}]_2$

Aldo Bianchini and Louis J. Farrugia*

Department of Chemistry, The University, Glasgow G12 8QQ, Scotland, U.K.

Received July 22, 1991

The reaction of $HgPh_2$ with hydride-containing methoxymethylidyne precursors has led to the high-yield synthesis of $Hg[Fe_2M(\mu_3\text{-}COMe)(CO)_7(\eta\text{-}C_5H_5)]_2$ (**3**, M = Co; **4**, M = Rh) and $Hg[M_3(\mu\text{-}COMe)(CO)_{10}]_2$ (**5**, M = Fe; **6**, M = Ru). The trimercury cluster $Hg[Fe(CO)_4(\mu\text{-}Hg)Fe_3(\mu\text{-}COMe)(CO)_{10}]_2$ (**9**) is formed in low yield in the reaction leading to **5**. Crystal data for **3**: orthorhombic, space group *Pbca*, a = 16.572 (4) Å, b = 19.846 (3) Å, c = 20.224 (5) Å, V = 6651 (3) Å^3, R (R_w) = 0.030 (0.035) for 3783 independent absorption-corrected data to θ = 25°. Crystal data for **4**: monoclinic, space group $C2/c$, a = 25.293 (11) Å, b = 9.084 (3) Å, c = 15.541 (5) Å, β = 100.97 (3)°, V = 3505 (2) Å^3, R (R_w) = 0.041 (0.044) for 1564 independent absorption-corrected data to θ = 25°. Crystal data for **6**: monoclinic, space group $P2_1/c$, a = 13.894 (3) Å, b = 16.828 (6) Å, c = 16.620 (4) Å, β = 109.86 (2)°, V = 3655 (2) Å^3, R (R_w) = 0.064 (0.065) for 2209 independent absorption-corrected data to θ = 20°. Crystal data for **9**: triclinic, space group $P\bar{1}$, a = 8.511 (2) Å, b = 8.941 (2) Å, c = 17.796 (3) Å, α = 79.10 (1)°, β = 75.86 (2)°, γ = 69.38 (2)°, V = 1221.0 (5) Å^3, R (R_w) = 0.054 (0.064) for 3422 independent absorption-corrected data to θ = 26°. The metal–metal connectivities differ in **3** and **4**, the latter having two Hg–Rh and two Hg–Fe bonds, while the former has four Hg–Fe bonds. ^{13}C and ^{199}Hg NMR studies show that cluster **4** undergoes a novel metal framework rearrangement in solution involving migration of the Hg atom around the Fe_2Rh triangle.

Introduction

Numerous mercury-containing transition-metal clusters have now been reported.[1-9] The propensity of mercury to adopt a linear or *pseudo*linear coordination geometry means that relatively few clusters having mercury incorporated into the polyhedral core are known.[2] Commonly observed coordination modes are the formally three-coordinate μ_2-HgX moiety (X = halide or ML_n unit such as $CpMo(CO)_3$) bridging an M–M edge,[3a-e,m,5a] or the formally four-coordinate μ_3-HgX moiety capping a M_3 face.[3f,j-l]

One interesting class of transition-metal–mercury clusters is that where a mercury atom(s) links together two cluster subunits.[4-9] This linkage may occur via a single Hg atom acting in a bis-μ_2 mode[4,5] or in a bis-μ_3 mode,[6,7] via a linear Hg_2 unit acting in a bis-μ_2 mode[7] or bis-μ_3 mode,[9] or more unusually via an Hg_3 triangle acting as the link.[8] These linked clusters have been synthesized either by reaction of Hg^{2+} or Hg_2^{2+} salts with cluster carbonylate anions[5,6a,8] or by chemical[6b,7] or electrochemical[9] reduction of clusters in the presence of mercury metal. In this article we describe a new method for synthesizing Hg-linked clusters from the reaction of $HgPh_2$ with clusters containing M(μ-H)M bonds, which proceeds with the elimination of benzene. The elimination reaction of $Ru_3(\mu\text{-}H)\{\mu_3\text{-}\eta^2\text{-}C{\equiv}C^tBu\}(CO)_9$ with HgPhX leading to an Ru(μ-HgX)Ru interaction has been previously described by Rosenberg et al.[3a] More recently Handler et al.[10] have described a similar synthetic route to compounds containing Hg–Pt bonds, from an elimination reaction between Pt hydrides and HgPh(OH). Part of this work has been previously communicated.[4]

Results and Discussion

The reaction of $HgPh_2$ with $Fe_2M(\mu\text{-}H)(\mu_3\text{-}COMe)(CO)_7(\eta\text{-}C_5H_5)$ (**1**, M = Co;[11] **2**, M = Rh[12]) in toluene at 90°

(1) Burlitch, J. M. In *Comprehensive Organometallic Chemistry*; Wilkinson, G., Stone, F. G. A., Abel, E. A., Eds.; Pergamon Press: Oxford, U.K., 1982; Vol. 6, p 983.
(2) (a) Bow, J. J.; van der Berg, W.; Schlebos, P. P. J.; Kanters, R. P. F.; Schoondergang, M. F. T.; Bosman, W. P.; Smits, J. M. M.; Beurskens, P. T.; Steggerda, J. J.; van der Sluis, P. *Inorg. Chem.* **1990**, *29*, 2971. (b) Jones, R. A.; Real, F. M.; Wilkinson, G.; Galas, A. M. R.; Hursthouse, M. B. *J. Chem. Soc., Dalton Trans.* **1981**, 126. (c) Ragosta, J. M.; Burlitch, J. M. *Organometallics* **1988**, *7*, 1469. (d) Deutscher, J.; Fadel, S.; Zeigler, M. L. *Angew. Chem., Int. Ed. Engl.* **1977**, *16*, 704.
(3) (a) Rosenberg, E.; King, K.; Fahmy, R.; Tiripicchio, A.; Camellini-Tiripicchio, M. *J. Am. Chem. Soc.* **1980**, *102*, 3626. (b) Rosenberg, E.; Ryckman, D.; Gellert, R. W.; Hsu, I. *Inorg. Chem.* **1986**, *25*, 194. (c) Rosenberg, E.; Wang, J.; Gellert, R. W. *Organometallics* **1988**, *7*, 1093. (d) Rosenberg, E.; Novak, B. *Inorg. Synth.* **1989**, *26*, 328. (e) Horwitz, C. P.; Holt, E. M.; Brock, C. P.; Shriver, D. F. *J. Am. Chem. Soc.* **1985**, *107*, 8136. (f) Wang, J.; Sabat, M.; Horwitz, C. P.; Shriver, D. F. *Inorg. Chem.* **1988**, *27*, 552. (g) Sharp, P. R. *Inorg. Chem.* **1986**, *25*, 4185. (h) Faraone, F.; Schiavo, S. L.; Bruno, G.; Bombieri, G. *J. Chem. Soc., Chem. Commun.* **1984**, 6. (i) Field, J. S.; Haines, R. J.; Meintjies, E.; Sigwarth, B.; van Rooyen, P. H. *J. Organomet. Chem.* **1984**, *268*, C43. (j) Braunstein, P.; Rosé, J.; Tiripicchio, A.; Tiripicchio-Camellini, M. *J. Chem. Soc., Chem. Commun.* **1984**, 391. (k) Mednikov, E. G.; Bashilov, V. V.; Sokolov, V. I.; Slovokhotov, Yu. L.; Struchkov, Yu. T. *Polyhedron* **1983**, *2*, 141. (l) Henly, T. J.; Shapley, J. R. *Organometallics* **1989**, *8*, 2729. (m) Reina, R.; Rossell, O.; Seco, M. *J. Organomet. Chem.* **1990**, *398*, 285.
(4) Farrugia, L. J. *J. Chem. Soc., Chem. Commun.* **1987**, 147.
(5) (a) Ermer, S.; King, K.; Hardcastle, K. I.; Rosenberg, E.; Manotti-Lanfredi, A. M.; Tiripicchio, A.; Tiripicchio-Camellini, M. *Inorg. Chem.* **1983**, *22*, 1339. (b) Hajela, S.; Novak, B.; Rosenberg, E. *Organometallics* **1989**, *8*, 468. (c) Gomez-Sal, M. P.; Johnson, B. F. G.; Lewis, J.; Raithby, P. R.; Syed-Mustaffa, A. B. *J. Organomet. Chem.* **1984**, *272*, C21.
(6) (a) Braunstein, P.; Rosé, J.; Tiripicchio, A.; Tiripicchio-Camellini, M. *Angew. Chem., Int. Ed. Engl.* **1985**, *24*, 767. (b) Yamamoto, Y.; Yamazaki, H.; Sakurai, T. *J. Am. Chem. Soc.* **1982**, *104*, 2329.
(7) Albinati, A.; Moor, A.; Pregosin, P. S.; Venanzi, L. M. *J. Am. Chem. Soc.* **1982**, *104*, 7672.
(8) (a) Fajardo, M.; Holden, H. D.; Johnson, B. F. G.; Lewis, J.; Raithby, P. R. *J. Chem. Soc., Chem. Commun.* **1984**, 24. (b) Bailey, P. J.; Johnson, B. F. G.; Lewis, J.; McPartlin, M.; Powell, H. R. *J. Chem. Soc., Chem. Commun.* **1989**, 1513. (c) Gade, L. H.; Johnson, B. F. G.; Lewis, J.; McPartlin, M.; Powell, H. *J. Chem. Soc., Chem. Commun.* **1990**, 111.
(9) Drake, S. R.; Barley, M. H.; Johnson, B. F. G.; Lewis, J. *Organometallics* **1988**, *7*, 806.
(10) Handler, A.; Peringer, P.; Müller, E. P. *J. Organomet. Chem.* **1990**, *389*, C23.
(11) Aitchison, A. A.; Farrugia, L. J. *Organometallics* **1986**, *5*, 1103.

0276-7333/92/2311-0540$03.00/0

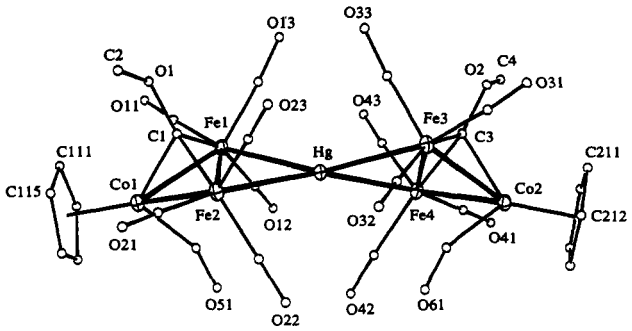

Figure 1. Molecular structure and atomic labeling scheme for $Hg[Fe_2Co(\mu_3\text{-}COMe)(CO)_7(\eta\text{-}C_5H_5)]_2$ (3).

Table I. Final Positional Parameters (Fractional Coordinates) with Esd's in Parentheses and Isotropic Thermal Parameters (Å²; Equivalent Isotropic Parameters U_{eq} for Anisotropic Atoms) for $Hg[Fe_2Co(\mu_3\text{-}COMe)(CO)_7(\eta\text{-}C_5H_5)]_2$ (3)[a]

atom	x/a	y/b	z/c	U_{eq}
Hg	0.60846 (2)	0.13373 (1)	0.11491 (1)	0.027
Fe(1)	0.69115 (6)	0.02147 (5)	0.15303 (5)	0.028
Fe(2)	0.55312 (6)	0.05349 (5)	0.21509 (5)	0.030
Fe(3)	0.51949 (7)	0.20759 (5)	0.02751 (6)	0.030
Fe(4)	0.67555 (6)	0.23888 (5)	0.04784 (6)	0.027
Co(1)	0.66246 (6)	−0.01358 (5)	0.26952 (5)	0.030
Co(2)	0.57359 (6)	0.32411 (5)	0.01272 (5)	0.027
O(1)	0.5781 (4)	−0.0882 (3)	0.1633 (3)	0.048
O(2)	0.6132 (3)	0.2239 (3)	−0.0907 (3)	0.044
O(11)	0.7977 (4)	−0.0941 (3)	0.1529 (4)	0.064
O(12)	0.8295 (4)	0.1163 (3)	0.1519 (4)	0.064
O(13)	0.6651 (5)	−0.0059 (4)	0.0127 (3)	0.070
O(21)	0.4550 (4)	−0.0005 (3)	0.3206 (3)	0.067
O(22)	0.5288 (5)	0.1931 (3)	0.2653 (3)	0.077
O(23)	0.4170 (4)	0.0400 (4)	0.1246 (4)	0.072
O(31)	0.4049 (4)	0.2489 (4)	−0.0724 (4)	0.070
O(32)	0.3982 (4)	0.2052 (4)	0.1364 (4)	0.078
O(33)	0.5112 (5)	0.0709 (3)	−0.0280 (4)	0.077
O(41)	0.7861 (4)	0.3419 (3)	0.0006 (4)	0.071
O(42)	0.7368 (4)	0.2559 (3)	0.1842 (3)	0.065
O(43)	0.7781 (4)	0.1321 (3)	−0.0034 (3)	0.056
O(51)	0.7092 (4)	0.1227 (3)	0.2828 (3)	0.056
O(61)	0.5516 94)	0.3104 (3)	0.1520 (3)	0.050
C(1)	0.6028 (4)	−0.0266 (3)	0.1858 (3)	0.028
C(2)	0.5046 (6)	−0.1171 (5)	0.1864 (5)	0.064
C(3)	0.6055 (4)	0.2362 (3)	−0.0259 (3)	0.026
C(4)	0.6868 (6)	0.2361 (5)	−0.1240 (5)	0.061
C(11)	0.7566 (5)	−0.0482 (4)	0.1539 (4)	0.041
C(12)	0.7753 (5)	0.0819 (4)	0.1524 (4)	0.040
C(13)	0.6735 (5)	0.0076 (4)	0.0675 (4)	0.044
C(21)	0.4966 (5)	0.0184 (4)	0.2808 (4)	0.043
C(22)	0.5395 (5)	0.1393 (5)	0.2447 (4)	0.048
C(23)	0.4708 (5)	0.0456 (5)	0.1583 (5)	0.052
C(31)	0.4490 (5)	0.2350 (4)	−0.0313 (5)	0.046
C(32)	0.4465 (5)	0.2052 (5)	0.0950 (4)	0.047
C(33)	0.5159 (6)	0.1242 (4)	−0.0041 (4)	0.049
C(41)	0.7414 (5)	0.3024 (4)	0.0183 (5)	0.045
C(42)	0.7110 (5)	0.2481 (4)	0.1335 (5)	0.045
C(43)	0.7381 (5)	0.1714 (4)	0.0174 (4)	0.035
C(51)	0.6818 (6)	0.0734 (4)	0.2649 (4)	0.047
C(61)	0.5657 (5)	0.3019 (4)	0.0964 (4)	0.042
C(111)	0.6932 (7)	−0.1130 (4)	0.2893 (4)	0.050
C(112)	0.7566 (4)	−0.0709 (3)	0.3080 (4)	0.062
C(113)	0.7284 (6)	−0.0275 (5)	0.3571 (2)	0.055
C(114)	0.6474 (6)	−0.0428 (2)	0.3687 (5)	0.046
C(115)	0.6257 (4)	−0.0956 (5)	0.3268 (3)	0.041
C(211)	0.5265 (7)	0.3711 (5)	−0.0698 (2)	0.056
C(212)	0.4865 (3)	0.3946 (4)	−0.0136 (5)	0.055
C(213)	0.5432 (7)	0.4256 (3)	0.0272 (4)	0.046
C(214)	0.6183 (5)	0.4213 (5)	−0.0036 (4)	0.049
C(215)	0.6080 (6)	0.3877 (2)	−0.0636 (5)	0.054

[a] $U_{eq} = {}^1/_3\sum_i\sum_j U_{ij}a_i^*a_j^*\mathbf{a}_i\cdot\mathbf{a}_j$.

C affords high yields of the dark green $Hg[Fe_2Co(\mu_3\text{-}COMe)(CO)_7(\eta\text{-}C_5H_5)]_2$ (3) or dark purplish brown $Hg[Fe_2Rh(\mu_3\text{-}COMe)(\mu\text{-}CO)(CO)_6(\eta\text{-}C_5H_5)]_2$ (4), respectively, as the sole isolable products. These mercury-linked clusters were characterized by spectroscopic techniques and by single-crystal X-ray diffraction studies. Discussion of their spectroscopic properties is deferred until their

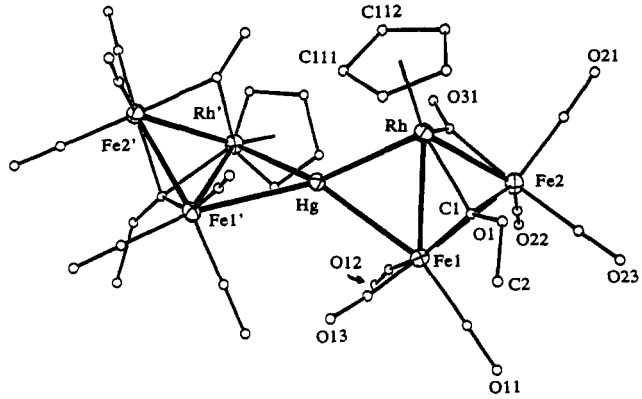

Figure 2. Molecular structure and atomic labeling scheme for $Hg[Fe_2Rh(\mu_3\text{-}COMe)(\mu\text{-}CO)(CO)_6(\eta\text{-}C_5H_5)]_2$ (4).

Table II. Selected Bond Lengths (Å) and Bond Angles (deg) for $Hg[Fe_2Co(\mu_3\text{-}COMe)(CO)_7(\eta\text{-}C_5H_5)]_2$ (3)

Hg–Fe(1)	2.727 91)	Hg–Fe(2)	2.735 (1)
Hg–Fe(3)	2.729 (1)	Hg–Fe(4)	2.726 (1)
Fe(1)–Fe(2)	2.685 (2)	Co(1)–Fe(1)	2.502 (2)
Fe(3)–Fe(4)	2.691 (2)	Co(2)–Fe(4)	2.494 (2)
Fe(1)–C(1)	1.868 (8)	Fe(2)–C(1)	1.886 (8)
Co(1)–C(1)	1.978 (7)	Fe(3)–C(3)	1.876 (7)
Fe(4)–C(3)	1.891 (8)	Co(2)–C(3)	1.984 (7)
Fe(1)–Hg–Fe(2)	58.9 (1)	Fe(1)–Hg–Fe(3)	153.3 (1)
Fe(1)–Hg–Fe(4)	124.1 (1)	Fe(2)–Hg–Fe(3)	127.7 (1)
Fe(2)–Hg–Fe(4)	162.0 (1)	Fe(3)–Hg–Fe(4)	59.1 (1)
Co(1)–C(51)–O(51)	154.1 (8)	Co(2)–C(61)–O(61)	156.0 (8)

Table III. Final Positional Parameters (Fractional Coordinates) with Esd's in Parentheses and Isotropic Thermal Parameters (Å²; Equivalent Isotropic Parameters U_{eq} for Anisotropic Atoms) for $Hg[Fe_2Rh(\mu_3\text{-}COMe)(\mu\text{-}CO)(CO)_6(\eta\text{-}C_5H_5)]_2$ (4)[a]

atom	x/a	y/b	z/c	U_{eq}
Hg	0.00000	−0.28895 (9)	0.25000	0.035
Rh	0.08570 (4)	−0.17928 (13)	0.36682 (7)	0.041
Fe(1)	0.10023 (9)	−0.42289 (21)	0.27028 (15)	0.045
Fe(2)	0.16846 (8)	−0.20446 (24)	0.29423 (13)	0.043
O(1)	0.1651 (5)	−0.3906 (16)	0.4513 (7)	0.086
O(11)	0.1821 (6)	−0.6293 (17)	0.2422 (12)	0.130
O(12)	0.0602 (6)	−0.4168 (18)	0.0806 (9)	0.109
O(13)	0.0391 (7)	−0.6458 (16)	0.3425 (12)	0.136
O(21)	0.2197 (6)	0.0702 (15)	0.3586 (10)	0.106
O(22)	0.1789 (6)	−0.1972 (15)	0.1109 (9)	0.096
O(23)	0.2669 (5)	−0.3656 (16)	0.3612 (10)	0.104
O(31)	0.0839 (5)	0.0030 (12)	0.2103 (7)	0.067
C(1)	0.1382 (6)	−0.3472 (18)	0.3743 (10)	0.052
C(2)	0.1696 (10)	−0.5380 (30)	0.4722 (16)	0.134
C(11)	0.1500 (8)	−0.5469 (20)	0.2533 (15)	0.083
C(12)	0.0730 (7)	−0.4103 (18)	0.1576 (14)	0.070
C(13)	0.0636 (7)	−0.5577 (18)	0.3073 (14)	0.074
C(21)	0.1997 (7)	−0.0362 (19)	0.3318 (11)	0.062
C(22)	0.1754 (7)	−0.2036 (21)	0.1812 (12)	0.069
C(23)	0.2290 (8)	−0.3043 (19)	0.3350 (12)	0.070
C(31)	0.1036 (6)	−0.0885 (16)	0.2619 (11)	0.050
C(111)	0.0136 (8)	−0.1192 (29)	0.4285 (10)	0.059
C(112)	0.0373 (5)	0.0111 (24)	0.4072 (13)	0.079
C(113)	0.0900 (8)	0.0154 (22)	0.4548 (6)	0.097
C(114)	0.0987 (6)	−0.1122 (30)	0.5055 (13)	0.105
C(115)	0.0515 (7)	−0.1954 (14)	0.4892 (10)	0.094

[a] $U_{eq} = {}^1/_3\sum_i\sum_j U_{ij}a_i^*a_j^*\mathbf{a}_i\cdot\mathbf{a}_j$.

(12) Farrugia, L. J. *J. Organomet. Chem.* **1986**, *310*, 67.

Table IV. Selected Bond Lengths (Å) and Bond Angles (deg) for $Hg[Fe_2Rh(\mu_3\text{-}COMe)(\mu\text{-}CO)(CO)_6(\eta\text{-}C_5H_5)]_2$ (4)

Hg–Rh	2.737 (2)	Hg–Fe(1)	2.775 (3)
Rh–Fe(1)	2.737 (3)	Rh–Fe(2)	2.570 (3)
Fe(1)–Fe(2)	2.609 (3)	Rh–C(1)	2.01 (2)
Fe(1)–C(1)	1.85 (2)	Fe(2)–C(1)	2.04 (2)
Rh–C(31)	1.96 (2)	Fe(2)–C(31)	1.93 (2)
Rh–Hg–Rh′	137.3 (1)	Rh–Hg–Fe(1)	59.5 (1)
Rh–Hg–Fe(1′)	145.7 (1)	Fe(1)–Hg–Fe(1′)	128.0 (1)
Rh–C(31)–O(31)	136 (1)	Fe(2)–C(31)–O(31)	141 (1)

structures have been described.

X-ray Crystal Structures of 3 and 4. The molecular structures and atomic labeling schemes for clusters 3 and 4 are shown in Figures 1 and 2, respectively. Atomic coordinates and important metrical parameters are given in Tables I–IV. In both cases the Hg atom replaces two hydrido ligands, linking together two Fe_2M triangles. The effective molecular symmetry in 3 and 4 is C_2, since the only symmetry element is a 2-fold rotation axis. This axis is crystallographically defined for 4 and is approximate for 3. Both metal cores are hence chiral, so that for cluster 3, the metal atoms Fe(1) and Fe(3) are chemically equivalent, as are Fe(2) and Fe(4), but these pairs are inequivalent to each other. The carbonyl ligands attached to these metals are hence potentially anisochronous.

The metal–metal connectivities in the two clusters differ. In both cases the Hg atom is four-coordinate, but in 3 the Hg atom bridges the Fe–Fe bond in both triangular subunits, while in 4 the Hg atom bridges an Fe–Rh bond in both triangular subunits. In the hydrido precursor species 1 and 2,[11,12] the hydride ligand bridges an Fe–Fe bond in both cases. The reason for these differing metal–metal connectivities is presumably the greater strength of an Hg–Rh bond versus that of an Hg–Fe bond, although the NMR studies reported below show than any energy difference must be very small. The Hg–Fe distances in 3 are virtually identical (range 2.726 (1)–2.735 (1) Å) and marginally shorter than found in 4, 2.775 (3) Å. These separations are longer than those found for the two- or three-coordinate mercury atoms in $[Fe(CO)_4(HgCl)(HgCl_2)]^-$ (Fe–Hg = 2.560) (3) and 2.516 (3) Å),[13] $(PPN^+)_2Hg[Fe(CO)_4]^{2-}$ (Fe–Hg = 2.547 (2) and 2.545 (2) Å),[14] and $(PPN^+)[Fe_4(CO)_{13}(\mu_3\text{-}Hg)Mo(CO)_3Cp]^-$ (Fe–Hg = 2.664 (1) and 2.686 (1) Å)[15] but somewhat shorter than those found for the asymmetrically bonded four-coordinate Hg atom in $(PPN^+)[Fe_4(CO)_{13}(\mu_3\text{-}HgCH_3)]^-$ (Hg–Fe = 2.606 (1), 2.847 (1), and 2.960 (1) Å).[16]

The angles at Hg show a wide range (58.9 (1)–162.0 (1)° for 3 and 59.5 (1)–145.7 (1)° for 4), and likewise the twist angle between the two HgM_2 planes differs substantially in the two clusters, viz. 46.2° in 3 and 71.9° in 4. The butterfly dihedral angles in 3 Hg–Fe(1)–Fe(2)–Co(1) = 153.7 (1)° and Hg–Fe(3)–Fe(4)–Co(2) = 152.3 (1)° are more obtuse than in 4, where Hg–Rh–Fe(1)–Fe(2) = 135.9 (1)°. In view of these distortions, and the facile rotation of the two subunits about the Hg atom (see below), we believe it inappropriate to view the coordination of the Hg atom as "tetrahedral" or "square planar" but regard it as *pseudo*linear in both cases. The two collinear Hg sp hybrids are involved in three-center–two-electron interactions with

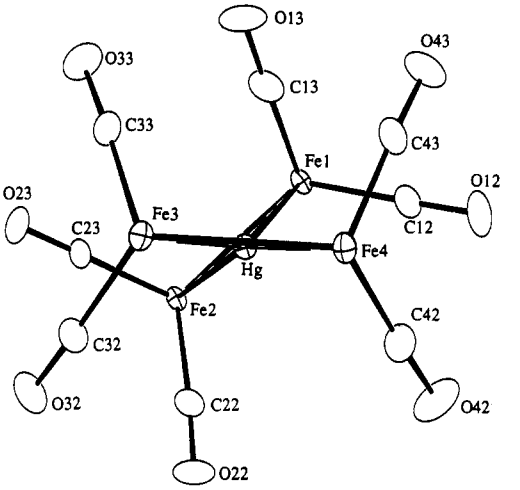

Figure 3. View down the MPT–Hg–MPT axis of 3, showing the arrangement of forward-pointing carbonyl ligands.

both bridged M–M vectors. This view is borne out by the near-linearity of the MPT–Hg–MPT angles (174.8° for 3 and 174.7° for 4, where MPT is the midpoint of the bridged M–M vector). The observed twist angle in the solid state is merely that which minimizes the nonbonding contacts between ligands on the two Fe_2M subunits. Thus, in 3, the observed conformation minimizes the interactions between the forward-pointing carbonyl oxygen atoms O(12), O(13), O(22), and O(23) on one subunit with those on the other subunit, viz. O(32), O(33), O(42), and O(43). This is illustrated in Figure 3, which shows a view down the MPT–Hg–MPT axis. A similar minimization of ligand interactions is observed in the other clusters reported in this article, and in previously reported bridged Hg clusters,[5a,c,6a] as well as related "naked" Ag[17] and Au-bridged[18] species.

The geometry within the $Fe_2Co(\mu_3COMe)(CO)_7Cp$ units in 3 closely resembles that found in the hydrido precursor 1.[11] In particular, the methoxymethylidyne ligand appears to have only a slightly increased interaction with the Co atoms; i.e., the Co(1)–C(1) and Co(2)–C(3) distances of 1.978 (7) and 1.984 (7) Å are marginally shorter than those found in 1 (2.001 (4) Å).[11] The usually observed[11] concomitant increase in the semi-μ_3 character of the carbonyls CO(51) and CO(61) is noted in the more acute Co–C–O angles in 3 (154.1 (8) and 156.0 (8)°) as compared with that in 1 (164.4 (4)°) and in the shorter Fe...C contacts (cf. 2.391 (9)–2.491 (9) Å in 3 versus 2.559 (4) and 2.629 (5) Å in 1[11]).

In contrast, the geometry of the $Fe_2Rh(\mu_3\text{-}COMe)(CO)_7Cp$ moieties in 4 and 2[12] differ markedly. In 2 the Rh-bound carbonyl is essentially linear (Rh–C–O = 169.1 (4)°)[12] and is uninvolved in bonding to the Fe atoms, while in 4 there is a carbonyl which symmetrically bridges one Rh–Fe bond, with Rh–C(31) = 1.96 (2) Å and Fe(2)–C(31) = 1.93 (2) Å. In addition, in 4 the methoxymethylidyne ligands caps the Fe_2Rh face somewhat asymmetrically (Fe(1)–C(1) = 1.85 (2) Å, Fe(2)–C(1) = 2.04 (2) Å, and Rh–C(1) = 2.01 (2) Å), while in 2 there is a weaker interaction with the Rh atom (Rh–C = 2.221 (4) Å).[12]

Finally, there are some short $Hg–C_{carbonyl}$ contacts, 2.861 (8)–2.890 (8) Å in 3 and 2.77 (2) and 2.97 (2) Å in 4, which may indicate weak Hg–C interactions. This phenomenon has been noted previously[14] and ascribed to a donation of

(13) Brotherton, P. D.; Kepert, D. L.; White, A. H.; Wild, S. B. *J. Chem. Soc., Dalton Trans.* **1976**, 1870.
(14) Alvarez, S.; Ferrer, M.; Reina, R.; Rossel, O.; Seco, M.; Solans, X. *J. Organomet. Chem.* **1989**, *377*, 291.
(15) Wang, J.; Sabat, M.; Horwitz, C. P.; Shriver, D. F. *Inorg. Chem.* **1988**, *27*, 552.
(16) Horwitz, C. P.; Holt, E. M.; Brock, C. P.; Shriver, D. F. *J. Am. Chem. Soc.* **1985**, *107*, 8136.
(17) Fajardo, M.; Gomez-Sal, M. P.; Holden, H. D.; Johnson, B. F. G.; Lewis, J.; McQueen, R. C. S.; Raithby, P. R. *J. Organomet. Chem.* **1984**, *267*, C25.
(18) Johnson, B. F. G.; Kaner, D. A.; Lewis, J.; Raithby, P. R. *J. Chem. Soc., Chem. Commun.* **1981**, 753.

Table V. ^{199}Hg NMR Data at 35.8 MHz

complex (isomer)	chem shift, δ^a	mult	J(Rh–Hg), Hz	$\omega_{1/2}$, Hz
3 (I)	891[b]	s		60
	803[c]	s		100
4 (I)	848[d]	s		350[e]
4 (II)	588[d]	d	279	150 (360)[f]
4 (III)	138[d]	t	333	87 (145)[f]
4 (IV)	54[d]	t	290	85 (160)[f]

[a] Chemical shifts to high frequency; Ξ = 17.910 841 MHz (δ-($HgMe_2$) = 0) in CD_2Cl_2. [b] 223 K. [c] 298 K. [d] 213 K. [e] Signal not observed at 64.5 MHz. [f] Line widths at 64.5 MHz in parentheses.

electron density from the Hg–M bond to CO π^* orbitals.

NMR Studies on 3 and 4. The two collinear sp hybrids of the Hg^{2+} cation are isolobally related to the H^+ 1s orbital, and this explains the geometric relationship observed between the hydrido and mercurio clusters 1 and 3. In a recent MO study on $[Hg\{Fe(CO)_4\}_2]^{2-}$, Alvarez et al.[14] show that the high-lying nature of the 6p AO's of the mercury atom results in very little π character to the Fe–Hg bond. The electronic barrier to rotation about the M–Hg–M axis should thus be negligible, with steric factors dominating. Rosenberg et al.[3b] have reported NMR evidence for free rotation about the central Hg–Ru bond in *cis*-$Ru(CO)_4\{(\mu_3\text{-}Hg)Ru_3(\mu_3\text{-}C_2{}^tBu)(CO)_9\}_2$, and since our original communication,[4] they have also reported[5b] the dynamic behavior of $Hg[Ru_3(\mu_3\text{-}C_2{}^tBu)(CO)_9]_2$, which implicates rotation about the Hg–Ru bonds.

Despite the fact that the solid-state structure shows a chiral metal skeleton, the ^{13}C NMR spectrum of 3 at 213 K closely resembles that of 1,[11] with only four signals in the carbonyl region at δ 230.9, 213.8, 209.8, and 205.1 (relative intensities 1:2:2:2). This implies that each subunit, and the cluster as a whole, has acquired an effective molecular mirror plane. In order to account for this observation, we postulate two simultaneous fluxional processes, both of which must be rapid at 213 K: (a) rotation of the methyl group about the C–O bond of the $COCH_3$ ligand (giving effective mirror symmetry *within* a cluster subunit) and (b) cluster core enantiomerization. We have discussed process a previously,[19] and process b can occur through either free rotation or a restricted oscillation of the two subunits about the MPT–Hg–MPT axis. We have recently characterized a similar enantiomerization process in the platinum bridged cluster $Pt[Ru_3(\mu\text{-}H)(\mu_3\text{-}C_2{}^tBu)(CO)_9]_2$.[20] The intensity 1 signal at δ 230.9 is assigned to the semi-μ_3 carbonyls CO(51) and CO(61). Interestingly, this is the only signal which shows a significant change in chemical shift, as compared with the corresponding signal in 1 (which occurs at δ 214.7). The shift to high frequency is consistent with the greater μ_3 character of this ligand in 3 as compared with that in 1. The ^{199}Hg NMR spectrum of 3 shows a broad, temperature-dependent, singlet resonance (see Table V).

The NMR spectra of 4 are more interesting and indicate that there are several exchanging isomeric species in solution. The ^{199}Hg spectra (see Table V and Figure 4) provide the clearest indication of the nature of these isomers. At 213 K the four signals at δ 848, 588, 138, and 54 are attributed, on the basis of multiplicities due to ^{103}Rh coupling, to the isomers I–IV respectively shown in Chart I. These are present in the ratio of ca. 1:10:6:2, on the basis of integration of the ^{199}Hg spectrum. Isomer I corresponds to the structure of the Co analogue 3, while the most abundant isomer, II, has one Fe_2Rh triangle bonded

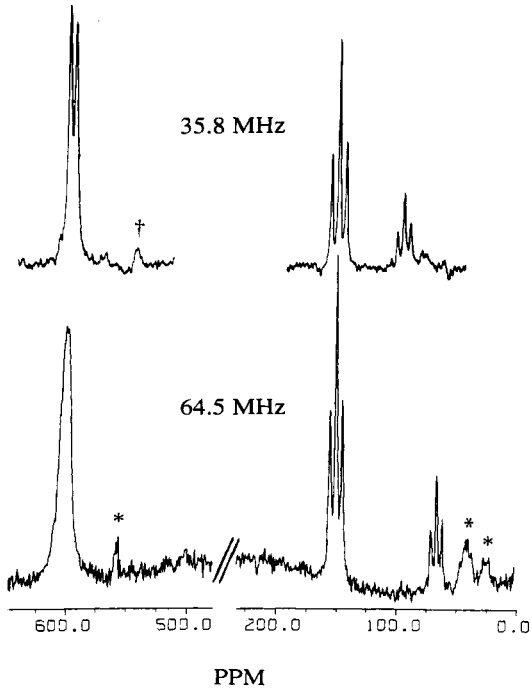

Figure 4. ^{199}Hg NMR spectra of 4 at 213 K. The asterisks (*) indicate impurities or unassigned minor isomers, and the signal marked with a dagger (†) is folded back from its genuine shift at δ 848.

Chart I

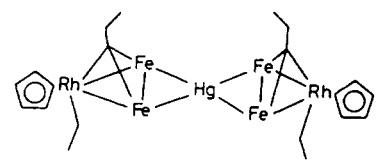

I

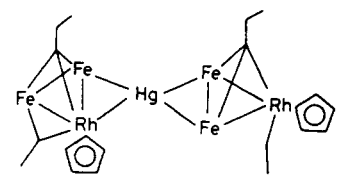

II

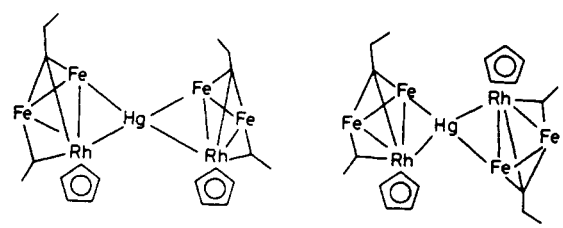

III IV

to the Hg atom via an Fe–Fe bond and the other triangle via an Fe–Rh bond. We attribute isomer III to the species 4 observed in the solid state and the less abundant isomer IV, which also has a triplet splitting due to (presumably) equivalent Rh nuclei, to a related species. This is possibly a rotamer of III (as shown), but it may also differ in the metal–ligand dispositions. When the temperature is increased from 213 K, all the signals broaden, and at ambient temperatures we were unable to detect any ^{199}Hg NMR resonances.

The variable-temperature ^{13}C spectra of 4 (^{13}CO enriched) in the CO region are shown in Figure 5. As ex-

(19) Aitchison, A. A.; Farrugia, L. J. *Organometallics* **1987**, *6*, 819.
(20) Farrugia, L. J. *Organometallics* **1990**, *9*, 105.

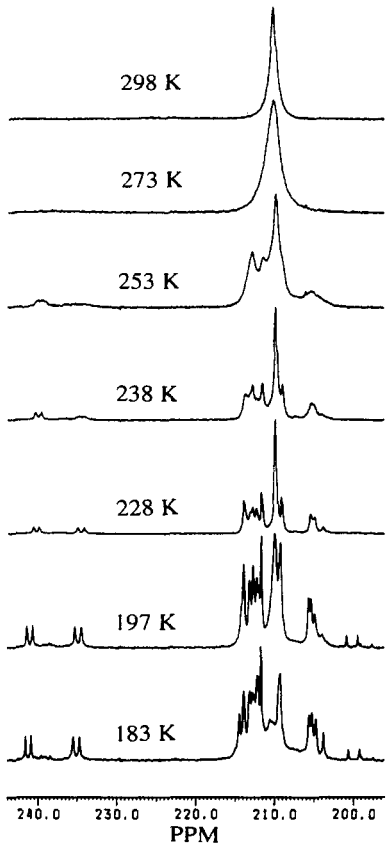

Figure 5. Variable-temperature ^{13}C NMR spectra of 4 in the carbonyl region.

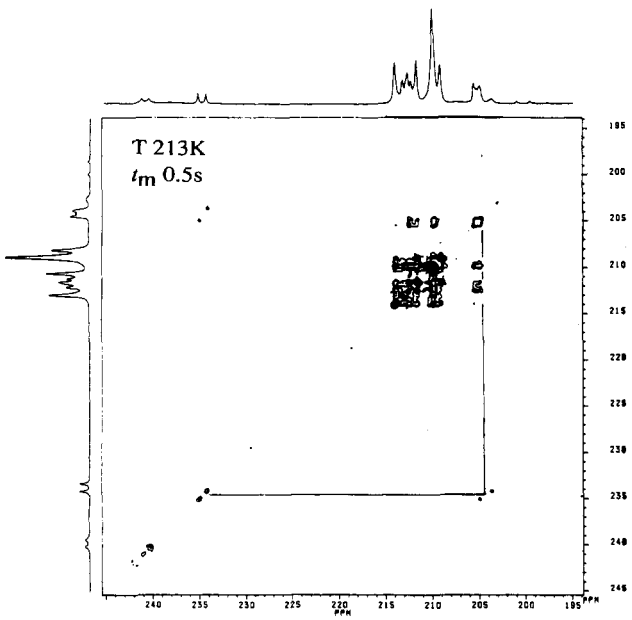

Figure 6. ^{13}C EXSY spectrum of 4 at 213 K in the carbonyl region.

pected, they are quite complex, and the complete carbonyl scrambling observed at 298 K is further confirmation of interisomer exchange. At 183 K there are two relatively intense doublets at δ 241.3 (J(Rh–C) = 37 Hz) and δ 235.1 (J(Rh–C) = 41 Hz), which are attributed to the bridging carbonyls in isomer III and isomer II, respectively, on the basis of intensities and the following observations. When the temperature is raised to 238 K, the lower frequency doublet resonance broadens faster than the higher frequency one, and a 2D-EXSY spectrum at 213 K, with a

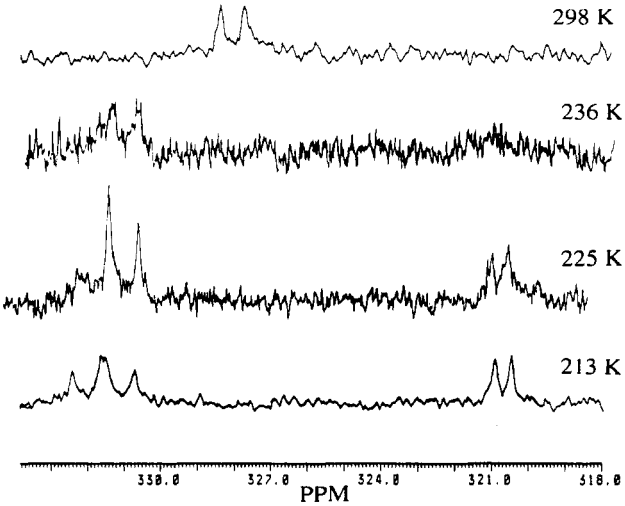

Figure 7. Variable-temperature ^{13}C NMR spectra of 4 in the alkylidyne region.

Scheme I

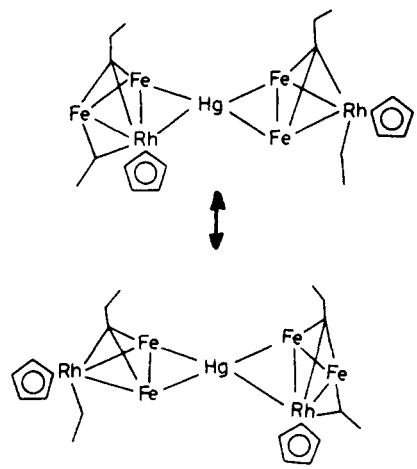

mixing time t_m of 0.5 s (Figure 6), shows that this low-frequency signal exchanges only with a doublet at δ 204.5 (J(Rh–C) = 75 Hz), which is attributed to the terminal Rh–CO in isomer II. This indicates that the two Fe_2Rh triangles in isomer II interchange their connectivities with the Hg atom, such that both triangular subunits become equivalent on the NMR time scale (see Scheme I). The barrier to this unusual degenerate exchange is slightly lower than, but comparable to, those for the nondegenerate exchanges between isomers. Further evidence for this exchange process comes from the temperature dependence of the alkylidyne ^{13}C signals shown in Figure 7. There are only three resonances visible, arising from the two most abundant isomers II and III. Two alkylidyne signals at δ 332.0 (J(Rh–C) = 40 Hz) and δ 320.7 (J(Rh–C) = 22 Hz), which are attributed to the two inequivalent $COCH_3$ groups in II, broaden faster than the third signal at δ 331.1 (J(Rh–C) = 40 Hz), which is ascribed to the two equivalent groups in III. At ambient temperatures only one signal is observed at the weighted mean chemical shift. In view of the well-known redistribution chemistry of mercury in cluster compounds,[3b,c,l] intermolecular exchange is a possibility. However, an equimolar mixture of 3 and 4 only showed NMR signals for the starting materials after 1 day; thus, an intermolecular exchange seems unlikely.

Unfortunately, the assignment of other carbonyl signals in Figure 5 is more difficult. From chemical shift comparisons with the precursor complex 2,[12] the set of resonances between δ 214.4 and 209.3 may be assigned to Fe-

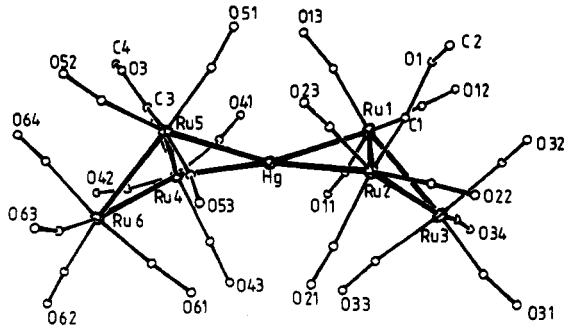

Figure 8. Molecular structure and atomic labeling scheme for $Hg[Ru_3(\mu\text{-}COMe)(CO)_{10}]_2$ (**6**).

bound carbonyls, while the signals between δ 205.6 and 199.9 can be ascribed to Rh-bound carbonyls. Tentatively we ascribe the doublet at δ 199.9 (J(Rh–C) = 71 Hz) to isomer I and remaining signals around δ 205 to II and IV.

Finally, some comment on the ^{199}Hg line widths given in Table V is merited. These were recorded at 213 K, at which temperature chemical exchange is slow. Although we have not measured ^{199}Hg T_1 values for clusters **3** and **4**, they must be on the order of ~0.05 s or less, since we were able to acquire spectra using $\pi/2$ pulses with repetition times of 0.04 s. As T_2 cannot be any longer than T_1, the line widths reported herein are a reflection of short T_1 values. Relaxation of ^{199}Hg is thought to be dominated by the shielding anisotropy interaction, and since $\Delta\delta$ can be 3000–7500 ppm for linear Hg complexes, this mechanism is very efficient.[21] The increase in line width when B_0 is increased (Table V), which is particularly visible for the signal at δ ~600 in Figure 4, is consistent with a shielding anisotropy mechanism. The lack of observable ^{199}Hg satellites in the ^{13}C spectra may also be attributed to short T_1 values. The differences in line widths for the different isomers of **4** can be ascribed to differing tumbling rates and hence correlation times τ_c. The moments of inertia for the isomers follow the order I > II > III ≈ IV due to the distances of the Rh atoms from the Hg atom, and hence, the tumbling rates follow the inverse order. Rosenberg, Milone, and co-workers[22] have recently reported ^{199}Hg NMR spectra for a number of Hg-bridged clusters, and they attribute the wide variation in line widths they observe (35–345 Hz) to scalar coupling relaxation to directly bonded quadrupolar nuclei. While this mechanism may possibly contribute to T_2 in cluster **3** because of the quadrupolar ^{59}Co nuclei, it cannot be of relevance to **4** since all directly bound nuclei have $I = 0$ or $^1/_2$.

Structure of $Hg[Ru_3(\mu\text{-}COCH_3)(CO)_{10}]_2$ (6). The clusters $Hg[M_3(\mu\text{-}COCH_3)(CO)_{10}]_2$ (**5**, M = Fe; **6**, M = Ru) are easily synthesized in medium to high yield from similar reactions of $M_3(\mu\text{-}H)(\mu\text{-}COCH_3)(CO)_{10}$ (M = Fe, Ru) with $HgPh_2$ in toluene at 90 °C. The IR evidence (see Experimental Section) suggests that **5** and **6** adopt different structures in the solid state; in particular **5** shows a bridging carbonyl stretch at 1795 cm^{-1}, whereas **6** only shows terminal CO stretches. The ^{1}H NMR evidence implies equivalent $COCH_3$ groups for both complexes in solution, but due to poor solubility we were not able to obtain definitive ^{13}C NMR spectra. Unfortunately, clusters **5** and **6** crystallize as polycrystalline dendrites, and we were only able to obtain a rather poor quality single crystal for cluster **6**. Despite problems with the data, the X-ray analysis provides an unambiguous determination of the main structural details of **6**. The molecular structure and atomic

Table VI. Final Positional Parameters (Fractional Coordinates) with Esd's in Parentheses and Isotropic Thermal Parameters (Å^2; Equivalent Isotropic Parameters U_{eq} for Anisotropic Atoms) for $Hg[Ru_3(\mu\text{-}COMe)(CO)_{10}]_2$ (6)[a]

atom	x/a	y/b	z/c	U_{eq}
Hg	0.85651 (18)	0.14258 (8)	0.25427 (12)	0.022
Ru(1)	0.6869 (3)	0.1901 (2)	0.3002 (2)	0.026
Ru(2)	0.6532 (3)	0.1307 (2)	0.1315 (2)	0.025
Ru(3)	0.5488 (3)	0.0632 (2)	0.2356 (2)	0.032
Ru(4)	1.0562 (3)	0.1225 (2)	0.3751 (2)	0.024
Ru(5)	1.0264 (3)	0.1894 (2)	0.2089 (2)	0.021
Ru(6)	1.1648 (3)	0.0617 (2)	0.2703 (2)	0.031
O(1)	0.552 (3)	0.288 (2)	0.160 (2)	0.07 (1)
O(3)	1.151 (2)	0.282 (1)	0.357 (1)	0.022 (7)
O(11)	0.796 (3)	0.091 (2)	0.460 (2)	0.06 (1)
O(12)	0.537 (3)	0.255 (2)	0.374 (2)	0.07 (1)
O(13)	0.816 (3)	0.340 (2)	0.344 (2)	0.08 (1)
O(21)	0.751 (3)	−0.027 (2)	0.102 (2)	0.08 (1)
O(22)	0.458 (3)	0.099 (2)	−0.007 (2)	0.07 (1)
O(23)	0.745 (3)	0.227 (2)	0.022 (2)	0.07 (1)
O(31)	0.400 (3)	−0.063 (2)	0.125 (2)	0.08 (1)
O(32)	0.382 (3)	0.175 92)	0.164 (2)	0.08 (1)
O(33)	0.735 (3)	−0.050 (2)	0.291 (2)	0.07 (1)
O(34)	0.514 (3)	0.035 (2)	0.404 (2)	0.08 (1)
O(41)	0.968 (2)	0.217 (2)	0.488 (2)	0.045 (8)
O(42)	1.252 (3)	0.093 (2)	0.522 (2)	0.06 (1)
O(43)	0.965 (2)	−0.043 (2)	0.394 (2)	0.053 (8)
O(51)	0.898 (2)	0.337 (2)	0.166 (2)	0.050 (9)
O(52)	1.178 (3)	0.270 (2)	0.142 (2)	0.06 (1)
O(53)	0.922 (2)	0.090 (2)	0.042 (2)	0.052 (9)
O(61)	0.980 (2)	−0.044 (2)	0.197 (2)	0.052 (8)
O(62)	1.291 (3)	−0.070 (2)	0.378 (2)	0.07 (1)
O(63)	1.211 (3)	0.055 (2)	0.105 (2)	0.08 (1)
O(64)	1.333 (3)	0.186 (2)	0.349 (2)	0.060 (9)
C(1)	0.603 (3)	0.208 (2)	0.187 (2)	0.011 (9)
C(2)	0.510 (4)	0.307 (3)	0.070 (3)	0.06 (1)
C(3)	1.095 (3)	0.226 (2)	0.331 (2)	0.021 (9)
C(4)	1.193 (4)	0.296 (3)	0.453 (3)	0.06 (1)
C(11)	0.750 (3)	0.125 (2)	0.399 (2)	0.03 (1)
C(12)	0.597 (4)	0.229 (3)	0.349 (3)	0.05 (1)
C(13)	0.759 (4)	0.285 (3)	0.330 (3)	0.06 (2)
C(21)	0.717 (5)	0.025 (4)	0.116 (3)	0.08 (2)
C(22)	0.537 (3)	0.114 (2)	0.044 (2)	0.03 (1)
C(23)	0.712 (3)	0.194 (3)	0.066 (2)	0.04 (1)
C(31)	0.462 (4)	−0.021 (3)	0.169 (3)	0.04 (1)
C(32)	0.434 (5)	0.141 (3)	0.230 (3)	0.071 (9)
C(33)	0.671 (3)	−0.005 (2)	0.270 (2)	0.03 (1)
C(34)	0.532 (4)	0.052 (3)	0.346 (3)	0.07 (2)
C(41)	0.997 (3)	0.178 (2)	0.445 92)	0.020 (9)
C(42)	1.174 (3)	0.100 (2)	0.461 (2)	0.04 (1)
C(43)	0.999 (3)	0.020 (2)	0.386 (2)	0.03 (1)
C(51)	0.939 (3)	0.280 (2)	0.179 (2)	0.017 (9)
C(52)	1.123 (3)	0.234 (2)	0.167 (2)	0.03 (1)
C(53)	0.954 (3)	0.126 (2)	0.107 (2)	0.04 (1)
C(61)	1.055 (4)	−0.002 (3)	0.222 (3)	0.05 (1)
C(62)	1.247 (4)	−0.020 (3)	0.340 (3)	0.07 (2)
C(63)	1.196 (4)	0.048 (3)	0.171 (3)	0.05 (1)
C(64)	1.273 (3)	0.146 (2)	0.319 (2)	0.023 (9)

[a] $U_{eq} = {}^1/_3\sum_i\sum_j U_{ij}a_i^*a_j^*\mathbf{a}_i\cdot\mathbf{a}_j$.

Table VII. Selected Bond Lengths (Å) and Bond Angles (deg) for $Hg[Ru_3(\mu\text{-}COMe)(CO)_{10}]_2$ (6)

Hg–Ru(1)	2.828 (5)	Hg–Ru(2)	2.875 (4)
Hg–Ru(4)	2.839 (4)	Hg–Ru(5)	2.823 (5)
Ru(1)–Ru(2)	2.862 (5)	Ru(1)–Ru(3)	2.827 (6)
Ru(2)–Ru(3)	2.845 (5)	Ru(4)–Ru(5)	2.878 (5)
Ru(4)–Ru(6)	2.853 (5)	Ru(5)–Ru(6)	2.833 (5)
Ru(1)–C(1)	1.87 (4)	Ru(2)–C(1)	1.86 (4)
Ru(4)–C(3)	2.03 (4)	Ru(5)–C(3)	2.03 (4)
Ru(1)–Hg–Ru(2)	60.2 (2)	Ru(1)–Hg–Ru(4)	123.1 (2)
Ru(1)–Hg–Ru(5)	147.4 (2)	Ru(2)–Hg–Ru(4)	169.2 (2)
Ru(2)–Hg–Ru(5)	122.6 (2)	Ru(4)–Hg–Ru(5)	61.1 (1)

(21) Goodfellow, R. J. In *Multinuclear NMR*; Mason, J., Ed.; Plenum Press: New York, 1987; Chapter 26, pp 568–569.

(22) Hajela, S.; Rosenberg, E.; Gobetto, R.; Milone, L.; Osella, D. *J. Organomet. Chem.* **1989**, *377*, 85.

Table VIII. Final Positional Parameters (Fractional Coordinates) with Esd's in Parentheses and Isotropic Thermal Parameters (Å²; Equivalent Isotropic Parameters U_{eq} for Anisotropic Atoms) for $Hg[Fe(CO)_4(\mu\text{-}Hg)Fe_3(\mu\text{-}COMe)(CO)_{10}]_2$ (9)[a]

atom	x/a	y/b	z/c	U_{eq}
Hg(1)	0.00000	0.00000	0.00000	0.047
Hg(2)	−0.20882 (8)	0.01676 (7)	0.17956 (4)	0.042
Fe(1)	−0.2192 (3)	0.2421 (2)	0.0677 (1)	0.039
Fe(2)	−0.0284 (3)	−0.1729 (2)	0.2878 (1)	0.041
Fe(3)	−0.2957 (3)	−0.2350 (2)	0.2607 (1)	0.037
Fe(4)	−0.2782 (3)	−0.2118 (3)	0.4062 (1)	0.046
O(1)	0.0031 (14)	−0.5040 (12)	0.2662 (7)	0.060
O(11)	0.082 (2)	0.245 (2)	0.118 (1)	0.096
O(12)	−0.4667 (16)	0.4817 (16)	0.1637 (9)	0.089
O(13)	−0.197 (2)	0.458 (2)	−0.076 (1)	0.104
O(14)	−0.477 (2)	0.130 (2)	0.033 (1)	0.105
O(21)	−0.0694 (18)	0.1504 (15)	0.3256 (9)	0.094
O(22)	0.2074 (17)	−0.3274 (20)	0.3939 (8)	0.099
O(23)	0.2522 (17)	−0.1824 (15)	0.1544 (8)	0.076
O(31)	−0.224 (2)	−0.317 (2)	0.101 (1)	0.090
O(32)	−0.4117 (17)	−0.5100 (13)	0.3309 (8)	0.084
O(33)	−0.6431 (15)	−0.0003 (14)	0.2596 (9)	0.084
O(41)	−0.0923 (19)	−0.5566 (15)	0.4399 (8)	0.085
O(42)	−0.5956 (18)	−0.2635 (17)	0.4975 (8)	0.092
O(43)	−0.4591 (16)	0.1254 (14)	0.3593 (7)	0.068
O(44)	−0.1740 (19)	−0.1116 (17)	0.5284 (9)	0.094
C(1)	−0.0694 (19)	−0.3484 (16)	0.2733 (8)	0.039
C(2)	0.176 (2)	−0.584 (2)	0.274 (1)	0.073
C(11)	−0.035 (2)	0.241 (2)	0.097 (1)	0.058
C(12)	−0.364 (2)	0.385 (2)	0.126 (1)	0.049
C(13)	−0.202 (3)	0.374 (2)	−0.021 (1)	0.081
C(14)	−0.374 (2)	0.169 (2)	0.047 (1)	0.063
C(21)	−0.061 (2)	0.031 (2)	0.311 (1)	0.058
C(22)	0.114 (2)	−0.269 (2)	0.353 (1)	0.064
C(23)	0.139 (2)	−0.179 (2)	0.203 (1)	0.050
C(31)	−0.257 (2)	−0.282 (2)	0.163 (1)	0.056
C(32)	−0.369 (2)	−0.401 (2)	0.305 (1)	0.052
C(33)	−0.510 (2)	−0.085 (2)	0.262 (1)	0.058
C(41)	−0.159 (2)	−0.426 (2)	0.423 (1)	0.058
C(42)	−0.472 (2)	−0.244 (2)	0.462 (1)	0.062
C(43)	−0.380 (2)	−0.010 (2)	0.372 (1)	0.065
C(44)	−0.209 (2)	−0.154 (2)	0.480 (1)	0.062

[a] $U_{eq} = {}^1/_3\sum_i\sum_j U_{ij}a_i^*a_j^*\mathbf{a}_i\cdot\mathbf{a}_j$.

labeling scheme are shown in Figure 8, with atomic coordinates and important metrical parameters in Tables VI and VII, respectively.

Like **3** and **4**, cluster **6** has overall C_2 molecular symmetry and hence has a chiral metal core. The structure of each $Ru_3(\mu\text{-}COCH_3)(CO)_{10}$ subunit is similar to that determined for $Ru_3(\mu\text{-}H)(\mu\text{-}COCH_3)(CO)_{10}$[23] with an Hg atom replacing two hydrides and linking together two Ru_3 triangles. One minor difference is that the bridged Ru–Ru vectors are marginally longer than the nonbridged Ru–Ru vectors in the mercurio complex, while in the hydrido complex[23] they are indistinguishable. The $HgRu_6$ skeleton resembles that found in the related species $Hg[Ru_3(\mu\text{-}NO)(CO)_{10}]_2$ (**7**)[5c] and in $Hg[Ru_3(\mu_3\text{-}\eta^2\text{-}C_2{}^t\!Bu)(CO)_9]^2$ (**8**).[5a] The Hg–Ru bonds in **6** range from 2.823 (5) to 2.875 (4) Å, which compares with similar distances in **7** (2.868 (1) and 2.855 (1) Å)[5c] and **8** (2.808 (6)–2.840 (7) Å).[5a] The twist angle between the two $HgRu_2$ traingles is 45.5°. This angle is similar in **8** (44.6°)[5a] but is much smaller in **7** (27.6°).[5c] In contrast, the butterfly dihedral angles Hg–Ru(1)–Ru(2)–Ru(3) and Hg–Ru(4)–Ru(5)–Ru(6) in **6** (126.5 (2) and 129.1 (2)°, respectively) are very similar to those observed in **7** (123.3°)[5c] and **8** (124.4 and 126.7°).[5a]

As in complexes **3** and **4**, the Hg atom may be viewed as *pseudo*linear, since the MPT–Hg–MPT angle is 167.7°. One major difference, however, between clusters **6**, **7**, and **8** concerns the orientation of the Ru_3 triangles relative to the MPT–Hg–MPT axis. The geometry of cluster **6** may be described as cisoid, while the latter two are transoid.[24] The bridging $COCH_3$ groups in **6** are mutually cisoid, while the μ-NO groups in **7** and the μ_3-$C_2{}^t\!Bu$ groups in **8** are mutually transoid. In addition, the planes defined by the two Ru_3 triangles are crystallographically parallel in **7** and approximately so in **8**, while in **6** they are clearly not so. The different orientations adopted by the closely related clusters **6** and **7** in the solid are presumably a result of crystal-packing forces, since by extension of our results for **3** and **4**, the barrier to rotation of the Ru_3 triangles about the MPT–Hg–MPT axis is expected to be very low.

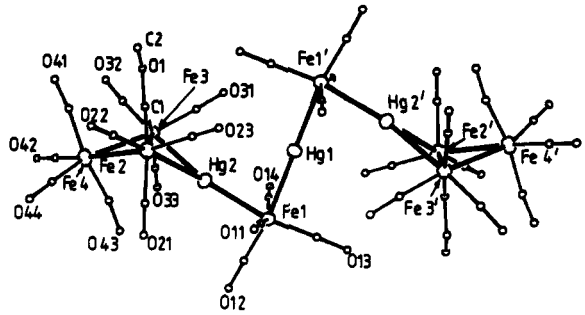

Figure 9. Molecular structure and atomic labeling scheme for $Hg[Fe(CO)_4(\mu\text{-}Hg)Fe_3(\mu\text{-}COMe)(CO)_{10}]_2$ (**9**).

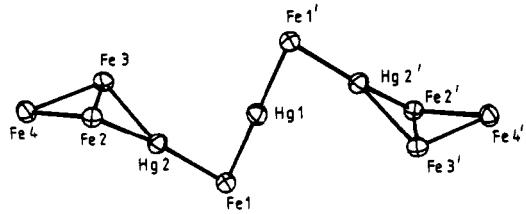

Figure 10. View of the unusual metal core geometry in **9**.

Table IX. Selected Bond Distances (Å) and Bond Angles (deg) for $Hg[Fe(CO)_4(\mu\text{-}Hg)Fe_3(\mu\text{-}COMe)(CO)_{10}]_2$ (9)

Hg(1)–Fe(1)	2.580 (2)	Fe(1)–Hg(2)	2.544 (3)
Hg(2)–Fe(2)	2.706 (3)	Hg(2)–Fe(3)	2.668 (3)
Fe(2)–Fe(3)	2.691 (3)	Fe(2)–Fe(4)	2.670 (4)
Fe(3)–Fe(4)	2.680 (4)	Fe(2)–C(1)	1.80 (1)
Fe(3)–C(1)	1.88 (2)	Hg(1)···Hg(2)	3.257 (1)
Fe(1)–Hg(2)–Fe(2)	145.3 (1)	Fe(1)–Hg(2)–Fe(3)	153.4 (1)
Fe(2)–Hg(2)–Fe(3)	60.1 (1)	Hg(1)–Fe(1)–Hg(2)	78.9 (1)
C(11)–Fe(1)–C(14)	159.6 (8)	C(12)–Fe(1)–C(13)	97.3 (9)

Structure of $Hg[Fe(CO)_4(\mu\text{-}Hg)Fe_3(\mu\text{-}COCH_3)(CO)_{10}]_2$ (9). During one preparation of cluster **5**, a few crystals of another complex, **9**, were isolated from the mother liquors. Although this complex is clearly only a very minor byproduct, we report it here because of its interesting structure. The molecular structure and atomic labeling scheme is shown in Figure 9, with atomic coordinates and important metrical parameters given in Tables VIII and IX, respectively. A view of the novel metal core is also given in Figure 10. The central Hg(1) atom lies on a crystallographic inversion center, so that the Fe(1)–Hg(1)–Fe(1′) angle is exactly 180°. Cluster **9** has exact C_i symmetry, and hence, in contrast to clusters **3**, **4**, and **6**, it is achiral. If the orientation of the methyl groups is ignored, the overall structure *approximates* to C_{2h}. The butterfly dihedral angle Hg(2)–Fe(2)–Fe(3)–Fe(4) is 127.9

(23) Churchill, M. R.; Beanan, L. R.; Wasserman, H. J.; Bueno, C.; Rahman, Z. A.; Keister, J. B. *Organometallics* **1983**, *2*, 1179.

(24) A rotation of one $HgRu_2$ triangle about the MPT–Hg–MPT axis, through the smallest angle necessary to bring the two $HgRu_2$ triangles into coplanarity, results in a cis arrangement for the bridging ligands in **6**, but a trans arrangement for the bridging ligands in **7** and **8**.

Table X. Experimental Data for Crystallographic Studies

	3	4	6	9
compd formula	$C_{28}H_{16}O_{16}Co_2Fe_4Hg$	$C_{28}H_{16}O_{16}Fe_4HgRh_2$	$C_{24}H_6O_{22}HgRu_6$	$C_{32}H_6O_{30}Fe_6Hg_3$
M_r	1150.26	1238.2	1453.3	959.4
space group	*Pbca*	*C2/c*	$P2_1/c$	$P\bar{1}$
cryst syst	orthorhombic	monoclinic	monoclinic	triclinic
a/Å	16.572 (4)	25.293 (11)	13.894 (3)	8.511 (2)
b/Å	19.846 (3)	9.084 (3)	16.828 (6)	8.941 (2)
c/Å	20.224 (5)	15.541 (5)	16.620 (4)	17.796 (3)
α/deg				79.10 (1)
β/deg		100.97 (3)	109.86 (2)	75.86 (2)
γ/deg				69.38 (2)
V/Å^3	6651 (3)	3505 (2)	3655 (2)	1221.0 (5)
Z	8	4	4	1
D_{calc}/g cm^{-3}	2.30	2.35	2.64	2.61
$F(000)$	4400	2344	2680	886
μ(Mo Kα)/cm^{-1}	73.41	69.47	66.35	117.83
θ range/deg	$2 < \theta < 25$	$2 < \theta < 25$	$2 < \theta < 20$	$2 < \theta < 26$
cryst size/mm	0.4 × 0.6 × 0.4	0.7 × 0.7 × 0.3	0.2 × 0.3 × 0.4	0.5 × 0.5 × 0.1
range of trans coeff cor	1.23/0.81	1.20/0.68	1.38/0.78	1.81/0.64
no. of data collected	7217	3370	5184	5129
no. of unique data	5823	3073	4747	4786
std rflns	$5\bar{9}6$, $\bar{9}52$	317, $8\bar{2}6$, $4\bar{2}6$	$\bar{4}29$, 3,0,$\overline{10}$	$\bar{2}4\bar{2}$, $\bar{5}0\bar{1}$
observability criterion n ($I > n\sigma(I)$)	2.0	2.0	3.0	3.0
no. of data in refinement	3783	1564	2209	3422
no. of refined params	382	222	246	331
final R	0.030	0.041	0.064	0.054
final R_w	0.035	0.044	0.065	0.064
largest remaining feature in electron density map/e Å^{-3}	+0.86, −0.62	1.04, −1.22	+3.6, −1.42	+2.04, −2.52
shift/esd in last cycle	0.01 (max), 0.001 (mean)	0.03 (max), 0.004 (mean)	0.16 (max), 0.07 (mean)	0.07 (max), 0.005 (mean)

(1)°. Two $Fe_3(\mu\text{-}COCH_3)(CO)_{10}$ units, whose structure closely resembles that found[25] in $Fe_3(\mu\text{-}H)(\mu\text{-}COCH_3)(CO)_{10}$ are linked by a "zigzag" Hg_3Fe_2 chain. This structure contains an extension of the type of linkage found in *cis*-$Ru(CO)_4\{(\mu_3\text{-}Hg)Ru_3(\mu_3\text{-}C_2{}^tBu)(CO)_9\}_2$ (**10**), in which two Ru_3 cluster units are linked by an Hg_2Ru chain.[3b] Similar $Tl\{\mu\text{-}Fe(CO)_4\}Tl$ cluster linkages are also found in anions such as $[Th_6Fe_{10}(CO)_{36}]^{6-}$, reported by Whitmire et al.[26]

The linking $Fe(CO)_4$ group shows an interesting distortion toward tetrahedral geometry. Thus, the C(12)–Fe(1)–C(13) and C(11)–Fe(1)–C(14) angles of 97.3 (9) and 159.6 (8)° are respectively wider and narrower than expected from regular octahedral geometry. The narrow Hg(2)–Fe(1)–Hg(1) angle of 78.9 (1)° results in a close Hg···Hg contact of 3.257 (1) Å. A similar distortion for the $Ru(CO)_4$ group occurs in **10**[3b] and in a number of main-group clusters containing $Fe(CO)_4$ units.[27,28] Elian and Hoffmann[29] have suggested that a tetrahedral distortion will occur in FeL_4X_2 complexes when the X group is strongly electron donating.

In an effort to extend the synthetic route to mercury-bridged clusters containing tetrahedral subunits, the reaction of $CoRu_3(\mu\text{-}H)(CO)_{13}$ with $HgPh_2$ in toluene was also investigated. However, there was extensive decomposition, and the only tractable product isolated was $Ru_6(\mu_6\text{-}C)(CO)_{14}(\eta^6\text{-}C_6H_5CH_3)$.[30] The failure to isolate the expected $Hg[CoRu_3]_2$ cluster may be attributed to steric congestion around the hydride-bridged $CoRu_2$ face in the precursor.[31] Henly and Shapley[31] also attribute steric congestion as one reason for the failure to isolate $[Hg\{Re_7C(CO)_{21}\}_2]^{4-}$.

Experimental Section

General experimental techniques and instrumentation were as previously described.[20] ^{199}Hg NMR spectra were recorded either at 35.8 MHz on a Bruker AM200SY instrument or at 64.5 MHz on a Bruker WH360 spectrometer and were acquired by using $\pi/2$ pulses with pulse repetition times of 0.01–0.04 s. ^{199}Hg chemical shifts are quoted to high frequency of Ξ = 17.910 841 MHz. The starting materials $Fe_2M(\mu\text{-}H)(\mu\text{-}COCH_3)(CO)_7Cp$ (M = Co,[11] Rh[22]) and $M_3(\mu\text{-}H)(\mu\text{-}COCH_3)(CO)_{10}$ (M = Fe, Ru[11]) were prepared as previously described, and $HgPh_2$ (Aldrich) was used as received.

Preparation of $Hg[Fe_2Co(\mu\text{-}COCH_3)(CO)_7(\eta\text{-}C_5H_5)]_2$ (3). To a solution of $Fe_2Co(\mu\text{-}H)(\mu\text{-}COCH_3)(CO)_7(\eta\text{-}C_5H_5)$ (0.2 g, 0.42 mmol) in toluene (20 mL), in a Schlenk tube fitted with a Teflon stopper, was added solid $HgPh_2$ (0.1 g, 0.27 mmol). The tube was sealed under 1 atm of nitrogen and placed in an oven at 90 °C for 12 h. Removal of the volatiles, and chromatography of the residue on Florasil in hexane, using hexane/dichloromethane mixtures as eluants, gave a single deep green band. Crystallization from hexane/dichloromethane mixtures at −20 °C afforded black crystals of the product $Hg[Fe_2Co(\mu\text{-}COCH_3)(CO)_7(\eta\text{-}C_5H_5)]_2$ (0.15 g, 62%).

By using exactly analogous procedures purple-brown **4** (55%), green **5** (63%), and deep orange-red **6** (58%) were obtained from $Fe_2Rh(\mu\text{-}H)(\mu\text{-}COCH_3)(CO)_7Cp$ and $M_3(\mu\text{-}H)(\mu\text{-}COCH_3)(CO)_{10}$ (M = Fe, Ru), respectively. In one large-scale preparation of **5** using 0.5 g of $Fe_3(\mu\text{-}H)(\mu\text{-}COCH_3)(CO)_{10}$ the reaction solution was cooled to room temperature and most of the poorly soluble complex **5** crystallized out. Concentration of the mother liquors afforded a further crop of **5**. When these mother liquors stood for 1 week, a few dark brown crystals (ca. 0.01 g) with a different morphology (platelike as opposed to dendritic clumps) were observed. These were found to be complex **9**. A ^{13}CO-enriched sample of **4** was prepared by heating a sample of **4** in toluene under 1 atm of ^{13}CO (99% ^{13}C) in a sealed vessel for 12 h and purifying by chromatography and recrystallization as described above.

Characterization Data (See Also Table V). Cluster 3: IR (CH_2Cl_2) ν(CO) 2054 (w), 2023 (s), 2017 (s, sh), 1991 (m), 1971 (m), 1829 (vw, br) cm^{-1}; ^1H NMR (CD_2Cl_2, 213 K) δ 5.36 (s, 10 H, Cp), 4.58 (s, 6 H, Me); ^{13}C NMR (CD_2Cl_2, 213 K) δ 320.3 (s, 2 C, *C*OMe), 230.9 (s, 2 C, Co–*C*O), 213.8 (s, 4 C, Fe–*C*O), 209.8

(25) Shriver, D. F.; Lehman, D.; Strope, D. *J. Am. Chem. Soc.* **1975**, *97*, 1594.
(26) Whitmire, K. H.; Cassidy, J. M.; Rheingold, A. L.; Ryan, R. R. *Inorg. Chem.* **1988**, *27*, 1347.
(27) Compton, N. A.; Errington, R. J.; Norman, N. C. *Adv. Organomet. Chem.* **1990**, *31*, 91.
(28) Campbell, C.; Farrugia, L. J. *Acta Crystallogr., Sect. C* **1989**, *C45*, 1817.
(29) Elian, M.; Hoffmann, R. *Inorg. Chem.* **1975**, *14*, 1058.
(30) Farrugia, L. J. *Acta Crystallogr., Sect. C* **1988**, *C44*, 1307.
(31) Farrugia, L. J. *Acta Crystallogr., Sect. C* **1988**, *C44*, 219.

(s, 4 C, Fe–CO), 205.1 (s, 4 C, Fe–CO), 90.7 (s, 10 C, Cp), 68.5 (s, 2 C, Me).

Cluster 4: IR (C_6H_{12}) ν(CO) 2060 (s), 2051 (vs), 2023 (vs), 2014 (vs), 2007 (sh), 1990 (m), 1982 (s), 1961 (m), 1955 (m), 1802 (m), 1787 (w) cm^{-1}; ^1H NMR (CD_2Cl_2, 298 K) δ 5.63 (d, 10 H, Cp, J(Rh–H) = 0.7 Hz), 4.34 (s, 6 H, Me); ^{13}C NMR (CD_2Cl_2, 298 K) δ 328.0 (s, br, 2 C, COMe), 210.5 (s, br, 14 C, CO), 94.0 (d, 10 C, Cp, J(Rh–C) = 2.0 Hz), 69.3 (s, 2 C, Me).

Cluster 5: IR (CH_2Cl_2) ν(CO) 2089 (w), 2071 (s), 2035 (vs), 2030 (sh), 2015 (s), 1989 (m), 1964 (sh), 1797 (vw, br) cm^{-1}; IR (KBr disk) 2965 (vw), 2858 (vw), 2090 (vs), 2075 (vs), 2040–1900 (vs, br, mult), 1795 (m), 1455 (s), 1280 (s), 1205 (m), 1161 (m), 915 (m), 788 (s), 584 (vs), 546 (sh), 490 (w), 463 (w), 439 (w), 415 (m), 330 (w) cm^{-1}; ^1H NMR ($CDCl_3$, 298 K) δ 4.80 (s, 3 H, Me).

Cluster 6: IR (KBr disk) 2960 (vw), 2855 (vw), 2100 (vs), 2085 (vs), 2060 (vs, br), 2040 (vs, br), 2010 (vs), 1995 (vs), 1981 (vs), 1965 (vs), 1454 (s), 1289 (vs), 1162 (w), 917 (m), 800 (s), 600 (m), 568 (vs), 546 (vs), 500 (m), 455 (m), 439 (m), 427 (m), 410 (vw), 390 (m), 322 (w) cm^{-1}; ^1H NMR ($CDCl_3$, 298 K) δ 4.75 (s, 3 H, Me).

Cluster 9: ^1H NMR ($CDCl_3$, 298 K) δ 4.64 (s, 6 H, Me). All complexes gave satisfactory C/H analyses.

Crystal Structure Analyses. Details of data collection procedures and structure refinement are given in Table X. Crystals of clusters **3**, **4**, and **6** were grown from hexane/dichloromethane mixtures, while the crystal of **9** was obtained from reaction mother liquors in toluene. Data were collected on an Enraf-Nonius CAD4F automated diffractometer, with graphite-monochromated X-radiation (λ = 0.710 69 Å). Unit cell parameters were determined by refinement of the setting angles ($\theta \geq 12°$) of 25 reflections. Data were collected at 298 K by using the $\theta/2\theta$ scan mode, and standard reflections were measured every 2 h during data collection. No decay correction was deemed necessary for clusters **6** and **9**, while linear corrections were applied to the data sets of **3** and **4** (3% and 15% decay, respectively). Lorentz–polarization and absorption corrections (DIFABS[32]) were applied to all data sets. One single crystal of cluster **6** was found after searching numerous potential candidates, but it diffracted poorly. In addition, we were only able to collect data to $\theta = 20°$, due to a catastrophic decay at this point. Systematic absences uniquely determined the space groups *Pbca* for **3** and $P2_1/c$ for **6** and indicated the space groups $C2/c$ (or Cc) and $P\bar{1}$ (or $P1$) for **4** and **9**, respectively. The distribution of normalized structure factors favored centrosymmetric space groups for the last two complexes. These choices were confirmed by successful solution and refinement for all structures. Structures were solved by direct methods (MITHRIL[33]) and subsequent electron difference syntheses. All non-hydrogen atoms were allowed anisotropic thermal parameters for clusters **3**, **4**, and **9**, while for **6** only the Ru and Hg atoms were refined with anisotropic thermal parameters. Hydrogen atoms were included at calculated positions for clusters **3**, **4**, and **9** with C–H = 1.0 Å and with fixed contributions to the structure factors (U = 0.08 Å^2). No hydrogen atoms were included for **6**. Refinement was by full-matrix least squares. The function minimized was $\sum w(|F_o| - |F_c|)^2$ with the weighting scheme $w = [\sigma^2(F_o)]^{-1}$ used and judged satisfactory. $\sigma(F_o)$ was estimated from counting statistics. Some light-atom positions for cluster **6** were poorly determined (for instance Ru(3)–C(32)–O(32) = 124.0°!); we attribute no physical significance to this but ascribe it to an artifact due to poor data quality. Nevertheless, the main structural features and cluster core geometry of **6** are satisfactorily determined by the X-ray analysis. Neutral atom scattering factors were taken from ref 34 with corrections for anomalous dispersion. All calculations were carried out on a MicroVAX 3600 computer using the Glasgow GX suite of programs.[35]

Acknowledgment. We thank Johnson-Matthey for a generous loan of Ru salts.

Note Added in Proof. The recently reported dynamic ^{13}C NMR spectra of $Hg[Os_3(\mu_3\text{-}C_2{}^t\text{Bu})(CO)_9]_2$[36] show mobility of the Hg atom, but with a much higher activation barrier than cluster **4**. Johnson and co-workers[37] have shown that the $Hg(CF_3COO)$ unit in $[Os_{10}C\{\mu\text{-}Hg(CF_3COO)\}(CO)_{24}]^-$ is highly mobile.

Registry No. **3**, 137946-89-5; **4**, 137946-90-8; **5**, 137965-28-7; **6**, 137965-29-8; **9**, 137946-91-9; $Fe_2CO(\mu\text{-}H)(\mu\text{-}COCH_3)(CO)_7(\eta\text{-}C_5H_5)$, 101224-54-8; $HgPh_2$, 587-85-9; $Fe_2Rh(\mu\text{-}H)(\mu\text{-}COCH_3)(CO)_7Cp$, 109661-50-9; $Fe_3(\mu\text{-}H)(\mu\text{-}COCH_3)(CO)_{10}$, 55992-19-3; $Ru_3(\mu\text{-}H)(\mu\text{-}COCH_3)(CO)_{10}$, 71737-42-3.

Supplementary Material Available: Tables of anisotropic thermal parameters and complete listings of bond lengths and angles for **3**, **4**, **6**, and **9** and listings of calculated hydrogen positional parameters for **3**, **4**, and **9** (22 pages); listings of calculated and observed structure factors for **3**, **4**, **6**, and **9** (38 pages). Ordering information is given on any current masthead page.

(32) Walker, N.; Stuart, D. *Acta Crystallogr., Sect. A* **1983**, *39A*, 158.
(33) Gilmore, C. J. *J. Appl. Crystallogr.* **1984**, *17*, 42.
(34) *International Tables for X-Ray Crystallography*; Kynoch Press: Birmingham, U.K., 1974; Vol. 4.
(35) Mallinson, P. R.; Muir, K. W. *J. Appl. Crystallogr.* **1985**, *18*, 51.
(36) Rosenberg, E.; et al. *Organometallics* **1991**, *10*, 203.
(37) Johnson, B. F. G. Private communication.